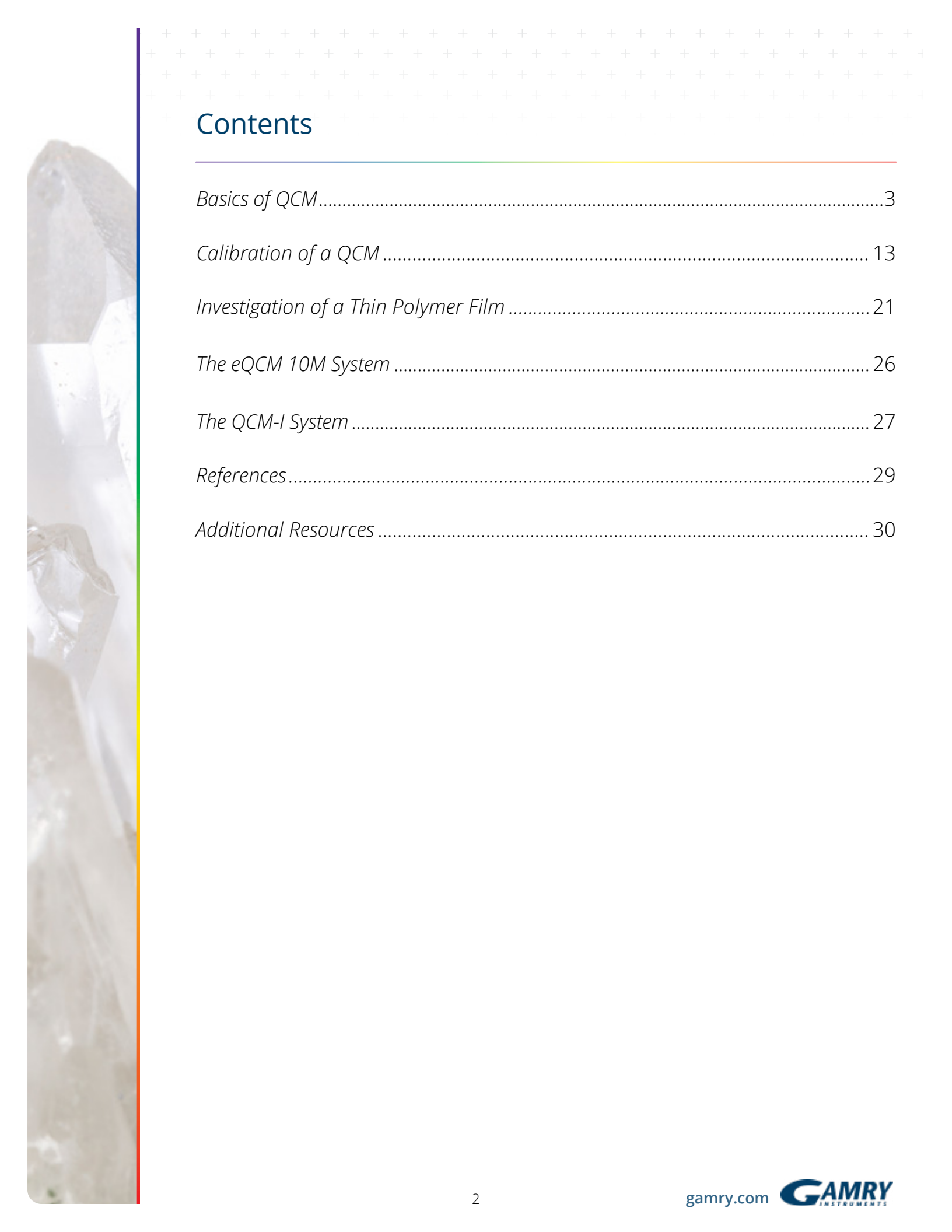


# Basics and Applications of a Quartz Crystal Microbalance Monitoring Surface Interactions via Small-scale Mass Changes

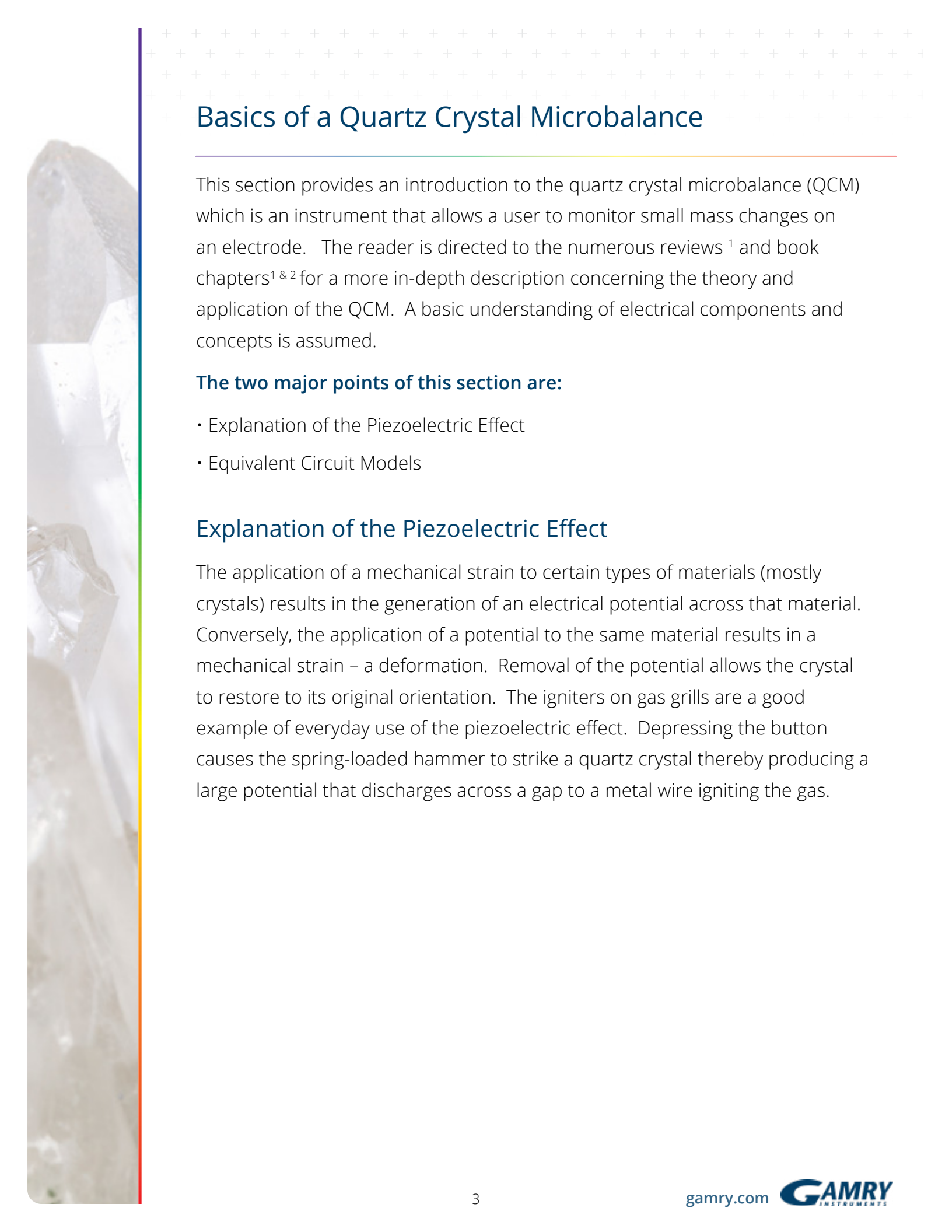




# Contents

---

<i>Basics of QCM</i> .....	3
<i>Calibration of a QCM</i> .....	13
<i>Investigation of a Thin Polymer Film</i> .....	21
<i>The eQCM 10M System</i> .....	26
<i>The QCM-I System</i> .....	27
<i>References</i> .....	29
<i>Additional Resources</i> .....	30



## Basics of a Quartz Crystal Microbalance

---

This section provides an introduction to the quartz crystal microbalance (QCM) which is an instrument that allows a user to monitor small mass changes on an electrode. The reader is directed to the numerous reviews<sup>1</sup> and book chapters<sup>1 & 2</sup> for a more in-depth description concerning the theory and application of the QCM. A basic understanding of electrical components and concepts is assumed.

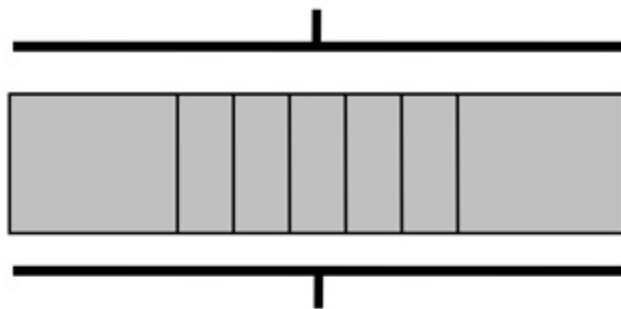
### **The two major points of this section are:**

- Explanation of the Piezoelectric Effect
- Equivalent Circuit Models

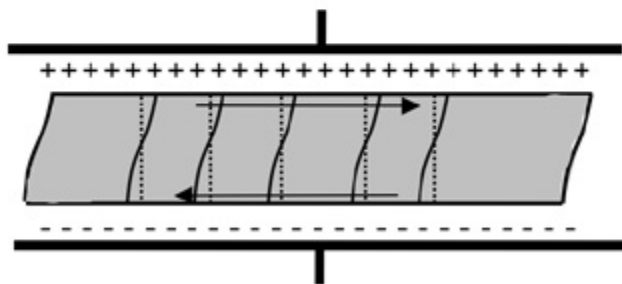
### **Explanation of the Piezoelectric Effect**

The application of a mechanical strain to certain types of materials (mostly crystals) results in the generation of an electrical potential across that material. Conversely, the application of a potential to the same material results in a mechanical strain – a deformation. Removal of the potential allows the crystal to restore to its original orientation. The igniters on gas grills are a good example of everyday use of the piezoelectric effect. Depressing the button causes the spring-loaded hammer to strike a quartz crystal thereby producing a large potential that discharges across a gap to a metal wire igniting the gas.

Quartz is by far the most widely utilized material for the development of instruments containing oscillators: partly due to historical reasons (the first crystals were harvested naturally), and partly due to its commercial availability (synthetically grown nowadays). There are many ways to cut quartz crystal and each cut has a different vibrational mode upon application of a potential. The AT-cut has gained the most use in QCM applications due to its low temperature coefficient at room temperature. This means that small changes in temperature only result in small changes in frequency. It has a vibrational mode of thickness shear deformation as shown below in Figure 1.



Quartz Crystal– No Applied Potential



Quartz Crystal– Under Applied Potential

**Figure 1.** Graphical Representation of Thickness Shear Deformation.

The application of an alternating potential (a sine wave in nearly all cases) to the crystal faces causes the crystal to oscillate. When the thickness of the crystal ( $t_q$ ) is twice the acoustical wavelength, a standing wave can be established where the inverse of the frequency of the applied potential is  $\frac{1}{2}$  of the period of the standing wave. This frequency is called the resonant frequency,  $f_0$ , and is given by equation 1:

$$f_0 = \sqrt{\frac{\mu_q}{\rho_q}} / 2t_q \quad 1$$

Where  $\mu_q$  is the shear modulus (a ratio of shear stress to shear strain),  $\rho_q$  is the density, and  $t_q$  is the crystal thickness. The amount of energy lost during oscillation at this frequency is at a minimum. The ratio of peak energy stored to energy lost per cycle is referred to as the quality factor,  $Q$  and is given by equation 2:

$$Q = \frac{f_c}{\Delta f_{FWHM}} \quad 2$$

where  $f_c$  is the center frequency and  $\Delta f_{FWHM}$  is the full width at half max. This full width at half max is also called the bandwidth. For quartz crystals in air,  $Q$  can exceed 100,000, while in solution,  $Q$  decreases to  $\sim 3000$ . This is because the crystal has been damped by the solution. This damping increases the amount of energy lost per cycle, decreasing  $Q$  as shown in Figure 2.

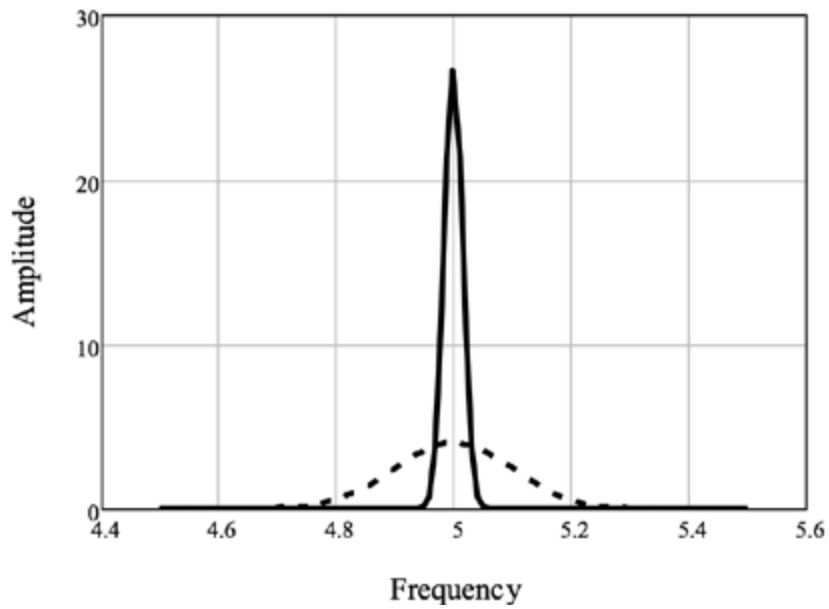


**Figure 2.** Comparison of High Q and Low Q.

### Equivalent Circuit Model

The mechanical model (Figure 3) of an electroacoustical system consists of a mass ( $M$ ), a compliance ( $C_m$ ), and a resistance ( $r_f$ ). The compliance represents energy stored during oscillation and the resistance represents energy dissipation during oscillation.

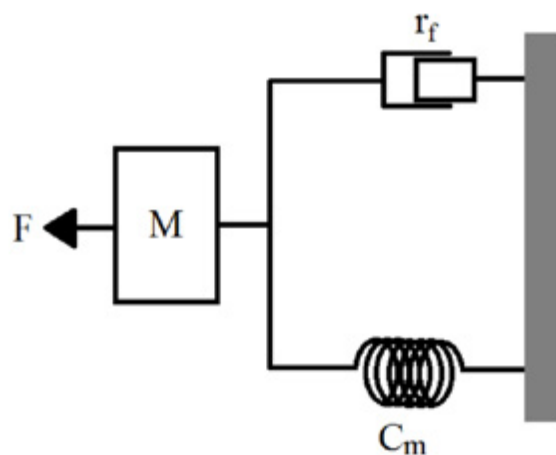


**Figure 3.** Quartz Crystal Microbalance Equivalent Mechanical Model.

The QCM mechanical model can be electrically modeled in several different ways. The easiest model to understand might be an RLC circuit as shown in Figure 4.



**Figure 4.** RLC Circuit.

Here  $R_1$  represents the energy dissipated during oscillation,  $C_1$  represents the energy stored during oscillation, and  $L_1$  represents the inertial component related to the displaced mass. At the resonant frequency,  $f_s$ , the impedance of the circuit is at a minimum and is equal in magnitude to  $R_1$  as shown in Figure 5.

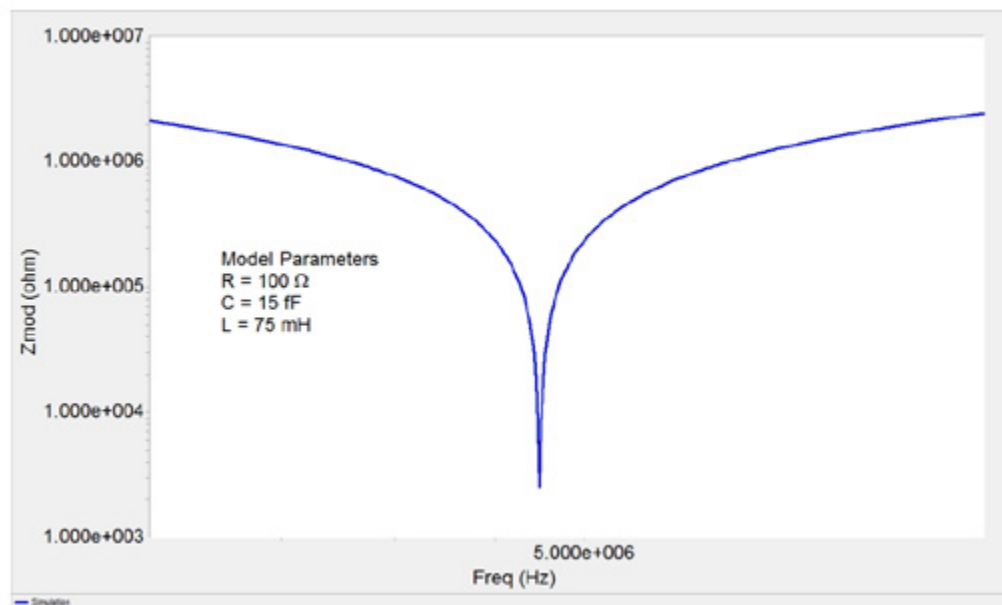


**Figure 5.** Impedance Spectrum for a Series RLC Circuit.

Here  $R_1$  represents the energy dissipated during oscillation,  $C_1$  represents the energy stored during oscillation, and  $L_1$  represents the inertial component related to the displaced mass. At the resonant frequency,  $f_s$ , the impedance of the circuit is at a minimum and is equal in magnitude to  $R_1$  as shown in Figure 5.

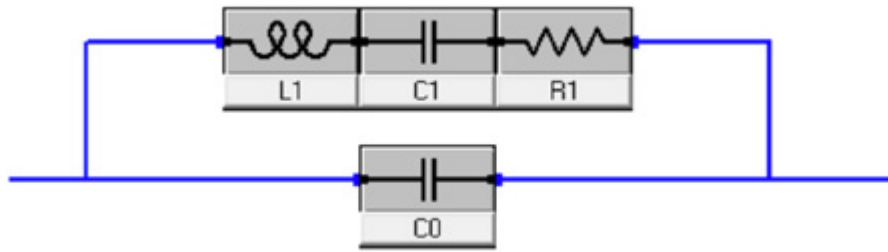


**Figure 6.** Butterworth – van Dyke (BvD) Equivalent Circuit Model.

The circuit shown above now has two resonant frequencies,  $f_s$  and  $f_p$ , which stand for the series resonant frequency (as in the original RLC circuit) and the parallel resonant frequency, respectively. The impedance spectrum for the BvD model is shown below with a minimum at  $f_s$  and a maximum at  $f_p$ .

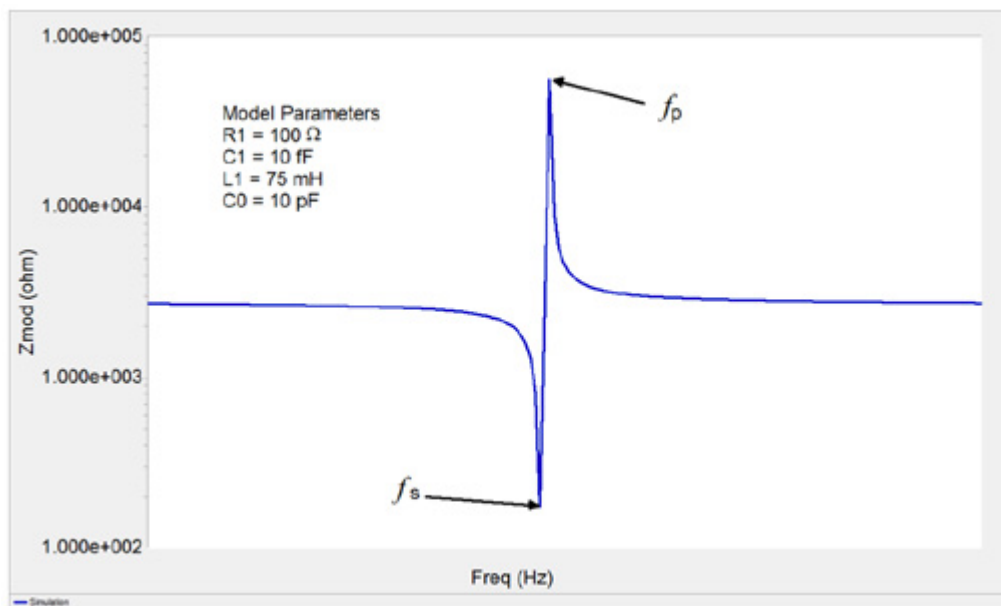


**Figure 7.** Impedance Spectrum for the BvD Equivalent Circuit Model.

Most commercial QCMs that rely upon a phase lock oscillator, manually cancel out  $C_0$ , and only report the series resonant frequency,  $f_s$  since  $f_s \approx f_0$  and  $f_s$  is obviously dependent upon  $L_1$ . The eQCM 10M reports both frequencies,  $f_s$  and  $f_p$ , and a relative impedance spectrum.

Since these two resonant frequencies are dependent upon  $L_1$ , mass changes on the surface of the electrode will result in frequency changes. When a deposited film is thin and rigid, the decrease in frequency can be directly correlated to the increase in mass using the Sauerbrey<sup>4</sup> equation 3.

$$\Delta f_s = -\frac{2f_0^2 mn}{(\mu_q \rho_q)^{1/2}} \quad 3$$

where  $f_0$  is the fundamental frequency of the crystal as defined in equation 1,  $m$  is the mass added,  $n$  is the harmonic number (e.g.  $n = 1$  for a 5 MHz crystal driven at 5 MHz), and  $\mu_q$  and  $\rho_q$  are as defined above. equation 3 can be reduced to:

$$\Delta f = -C_f m \quad 4$$

where  $C_f$  is the calibration constant. The calibration constant for a 5 MHz AT-cut quartz crystal in air is  $56.6 \text{ Hz cm}^2 \mu\text{g}^{-1}$  or  $226 \text{ Hz cm}^2 \mu\text{g}^{-1}$  for a 10MHz AT-cut crystal.

The majority of electrochemical experiments will correspond to a low-loading case, allowing you to directly correlate changes in frequency with changes in mass using the Sauerbrey equation 4.

Once a film has been deposited and the quartz crystal is immersed in a liquid, the BvD model can be modified as shown below to include coupling to the liquid.

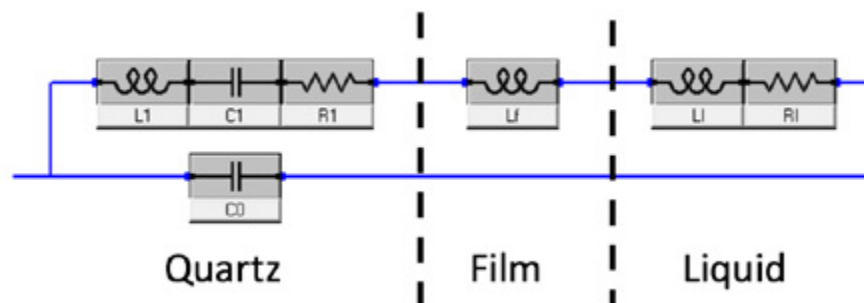


**Figure 8.** Equivalent Circuit Model for a Quartz Crystal Immersed in a Liquid

Three new components account for the mass loading of the film,  $L_f$ , and the liquid loading (based on  $\eta_L$  and  $\rho_L$ ),  $L_l$  and  $R_l$ . Both new mass loadings  $L_f$  and  $L_l$  have the effect of reducing the frequency as indicated with the black arrow in the chart below. The original BvD model (black curve) shows resonance approximately 300 kHz higher than the modified BvD model (red curve). Notice that the shapes of the resonance curves are identical despite the addition of the film and liquid loading.

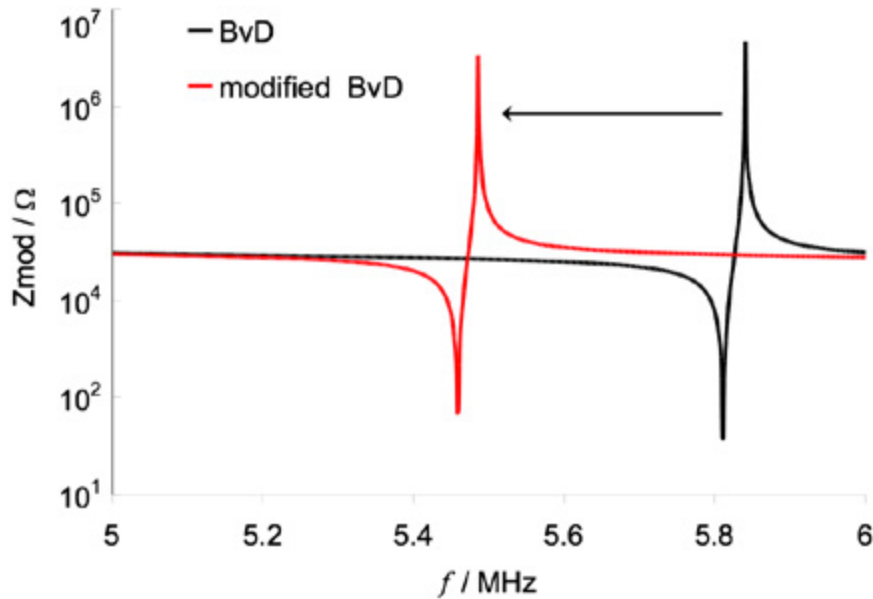


**Figure 9.** Comparison of BvD and Modified BvD Models.

Knowing the liquid's viscosity and density allows one to calculate<sup>3</sup> the expected frequency decrease upon immersing the crystal in that liquid using equation 5

$$\Delta f = -f_a^{3/2} \left( \frac{\eta_L \rho_L}{\pi \mu_q \rho_q} \right)^{1/2} \quad 5$$

where  $f_a$  is the frequency of the crystal in air,  $\eta_L$  is the viscosity of the liquid,  $\rho_L$  is the density of the liquid,  $\mu_q$  is the shear modulus of the quartz crystal, and  $\rho_q$  is the density of the quartz crystal.

For example, upon immersing the crystal in pure water, a frequency decrease of approximately 800 Hz is expected. Note  $f_a$  can be obtained using the eQCM 10M.

equation 4 holds as long as the film is assumed to be thin and rigid. When the film is no longer acoustically thin or is not rigid the BvD model can be modified further as shown below.

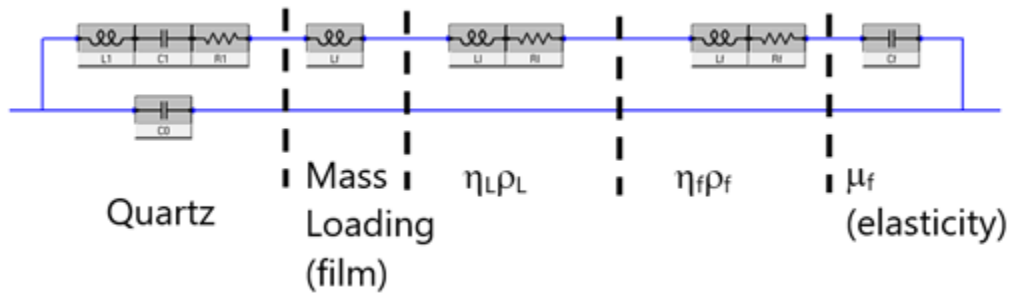


**Figure 10.** One Possible Equivalent Circuit Model for a Quartz Crystal Coated with a Polymer Film and Immersed in a Liquid

Two new features have been added – Film Loading ( $\eta_f \rho_f$ ) and Elasticity ( $\mu_f$ ). A viscoelastic polymer will influence the resonant frequencies based on the film's viscosity ( $\eta_f$ ), density ( $\rho_f$ ) and elasticity ( $\mu_f$ ). If the polymer is rigid or  $\eta_f \rho_f$  does not change during the experiment, there will be no change in peak shape and contributions from  $\eta_f \rho_f$  can be ignored. In cases where  $\eta_f \rho_f$  does change during the experiment, the frequency, magnitude and shape of the peak will also change as shown in Figure 11. These changes can be detected by looking at changes in  $f_p$  relative to  $f_s$ .

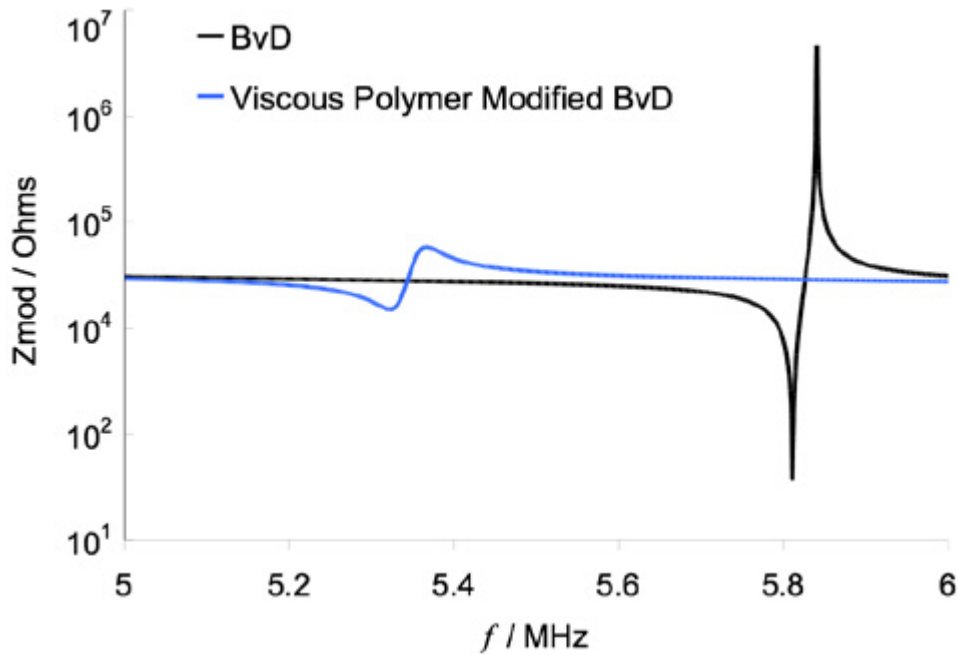
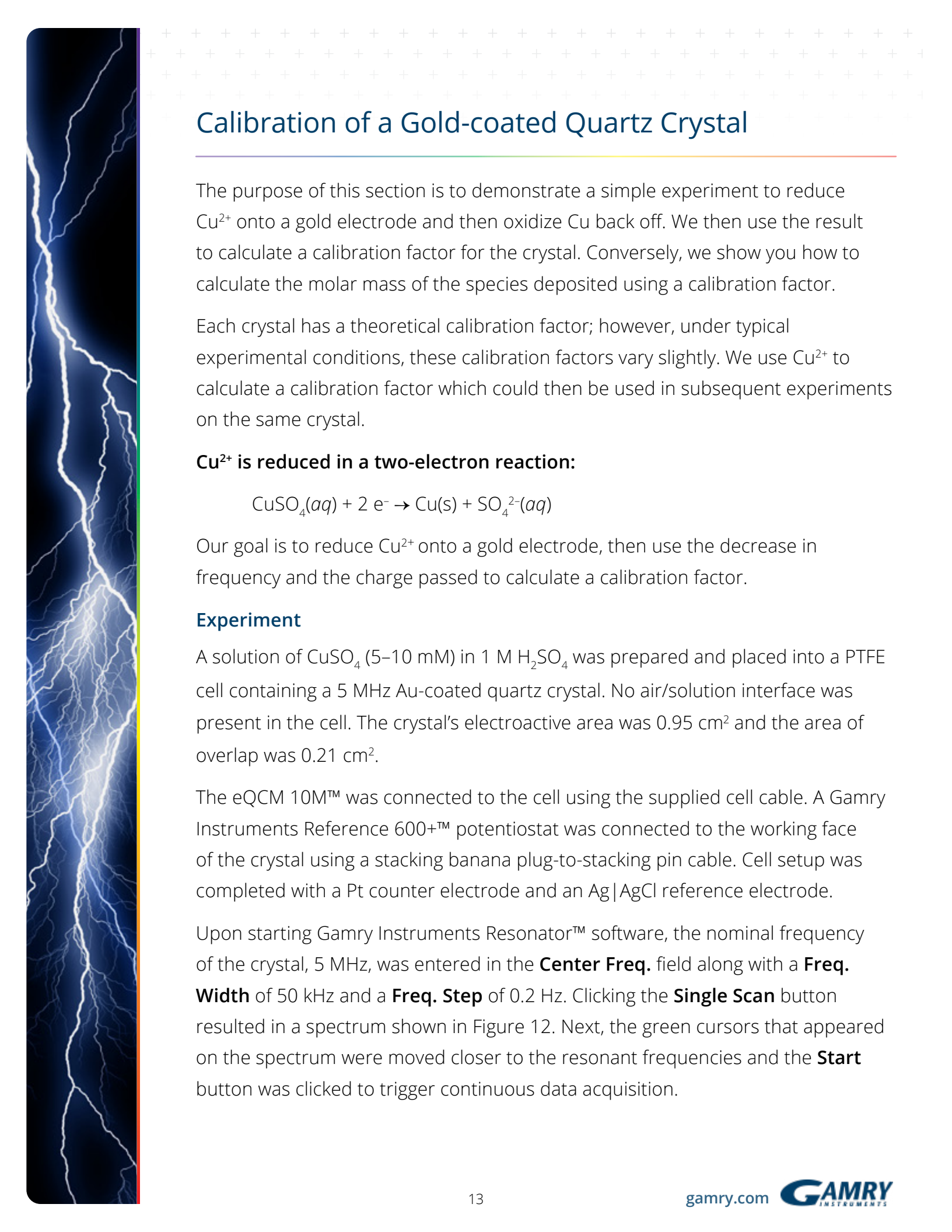


**Figure 11.** Comparison of BvD and Viscous Polymer Modified BvD Models.

Another way to visualize if  $\eta_f \rho_f$  is changing during an experiment is to look at the reduced quality factor,  $Q_R$  as a function of time (equation 6). The numerator is an estimate  $f_c$ . The denominator is an estimate of the bandwidth.

$$Q_R = \frac{(f_s + f_p) / 2}{(f_p - f_s)} \quad 6$$

Changes in  $Q_R$  correspond to changing  $\eta_f \rho_f$ . Quantifying changes in  $\eta_f \rho_f$  is challenging mathematically and will not be explored further here. The reader is directed to the literature<sup>5</sup> for additional information at this time.



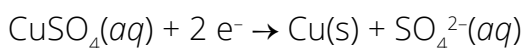
## Calibration of a Gold-coated Quartz Crystal

---

The purpose of this section is to demonstrate a simple experiment to reduce  $\text{Cu}^{2+}$  onto a gold electrode and then oxidize Cu back off. We then use the result to calculate a calibration factor for the crystal. Conversely, we show you how to calculate the molar mass of the species deposited using a calibration factor.

Each crystal has a theoretical calibration factor; however, under typical experimental conditions, these calibration factors vary slightly. We use  $\text{Cu}^{2+}$  to calculate a calibration factor which could then be used in subsequent experiments on the same crystal.

### **$\text{Cu}^{2+}$ is reduced in a two-electron reaction:**



Our goal is to reduce  $\text{Cu}^{2+}$  onto a gold electrode, then use the decrease in frequency and the charge passed to calculate a calibration factor.

### **Experiment**

A solution of  $\text{CuSO}_4$  (5–10 mM) in 1 M  $\text{H}_2\text{SO}_4$  was prepared and placed into a PTFE cell containing a 5 MHz Au-coated quartz crystal. No air/solution interface was present in the cell. The crystal's electroactive area was  $0.95 \text{ cm}^2$  and the area of overlap was  $0.21 \text{ cm}^2$ .

The eQCM 10M™ was connected to the cell using the supplied cell cable. A Gamry Instruments Reference 600+™ potentiostat was connected to the working face of the crystal using a stacking banana plug-to-stacking pin cable. Cell setup was completed with a Pt counter electrode and an Ag|AgCl reference electrode.

Upon starting Gamry Instruments Resonator™ software, the nominal frequency of the crystal, 5 MHz, was entered in the **Center Freq.** field along with a **Freq. Width** of 50 kHz and a **Freq. Step** of 0.2 Hz. Clicking the **Single Scan** button resulted in a spectrum shown in Figure 12. Next, the green cursors that appeared on the spectrum were moved closer to the resonant frequencies and the **Start** button was clicked to trigger continuous data acquisition.

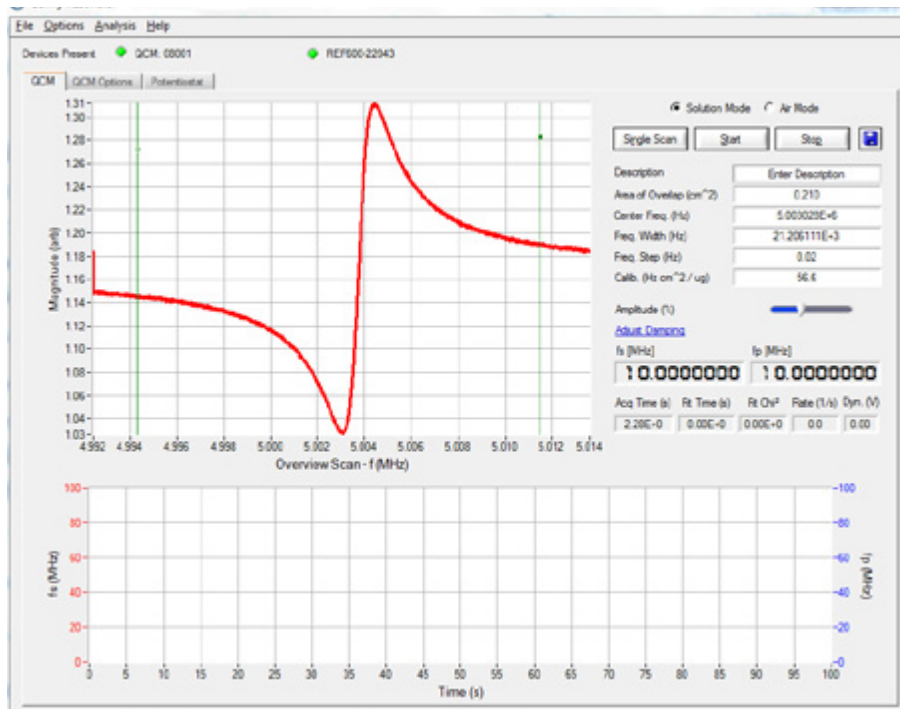


**Figure 12.** Resonator screenshot after entering initial parameters and clicking the **Single Scan** button.

The potentiostat was set up by selecting **Cyclic Voltammetry** from the **Technique** drop-down menu and clicking the **Setup** button. A setup screen for cyclic voltammetry appeared and parameters were entered as shown in Table 1:

Initial E (V):	0.050
Scan Limit 1 (V):	-0.250
Scan Limit 2 (V):	0.300
Final E (V):	0.050
Scan Rate (mV/s):	50
Step Size (mV):	2
Cycles (#):	5
I/E Range Mode:	Fixed
Max Current (mA):	30
Sampling Mode:	Surface

**Table 1**

After the potentiostat was set up, the **OK** button was clicked (which closed the setup window), followed by the **Run** button.

A screenshot of the potentiostat panel in Resonator during acquisition is shown in Figure 13. Note that the top plot shows the series of resonant frequencies for the entire time that the QCM has been acquiring data, while the bottom plot shows current and voltage data. It is also possible to show current and voltage versus time by selecting **Time** in the Display Graph drop-down menu.

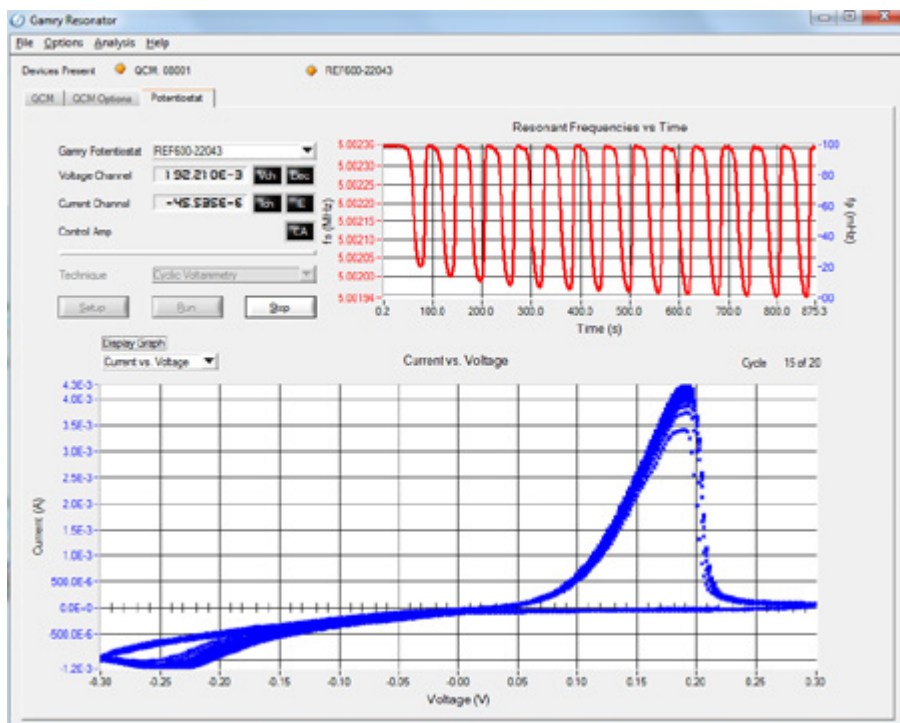


**Figure 13.** Screenshot of Resonator during acquisition.

After the acquisition was finished, the data file was then opened in Gamry Instruments' Echem Analyst™ software.

### Data Analysis

The first plot in Echem Analyst is a plot of the change in current and frequency versus voltage (Figure 14) and the second plot is change in frequency versus charge (Figure 15).

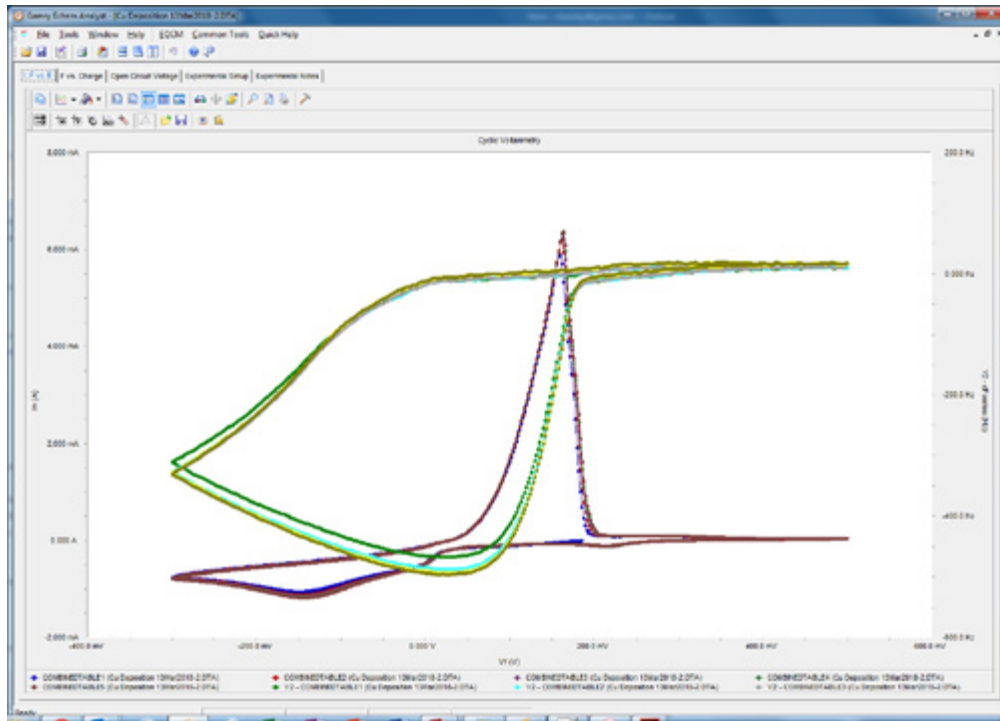


**Figure 14.** Echem Analyst™ showing change in current and frequency versus voltage for the five cycles.

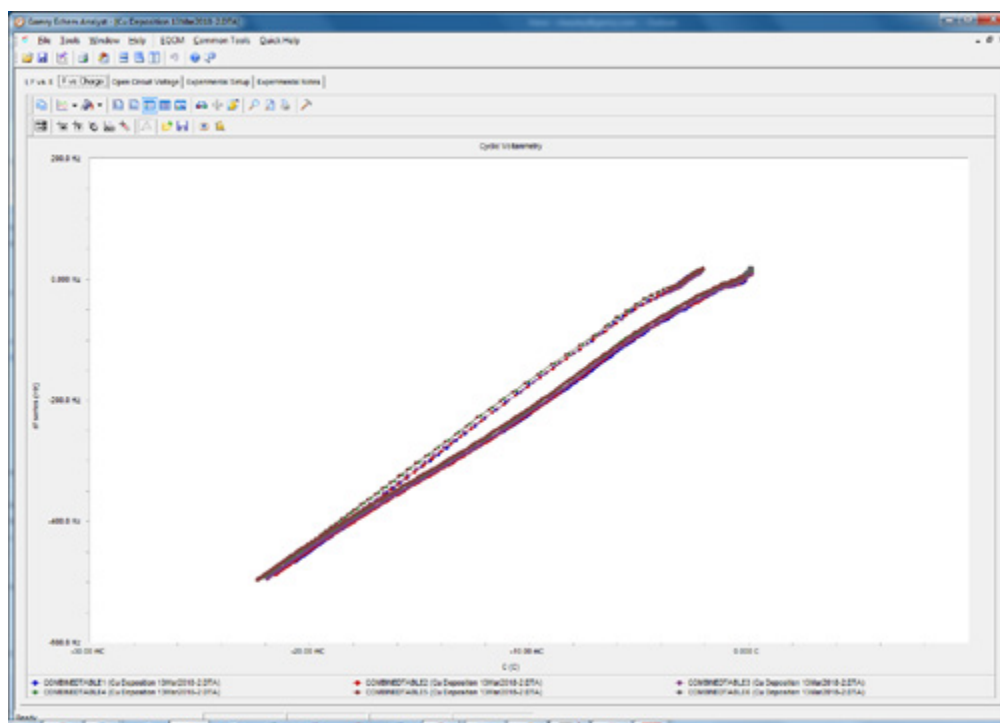


**Figure 15.** Echem Analyst™ showing change in current and frequency versus voltage for the five cycles.

Use the **Curve Selector** button  to plot data a variety of ways and also to show or hide specific curves. The deposition portion of the curve was selected by clicking on the **Select Portion of the Curve using the Mouse tool** button . A linear fit was then calculated by choosing the **Linear Fit** option under the **Common Tools** menu. The **Quick View** pane at the bottom of the window in Figure 16 gives the slope of the linear fit as 23.94 kHz/C.

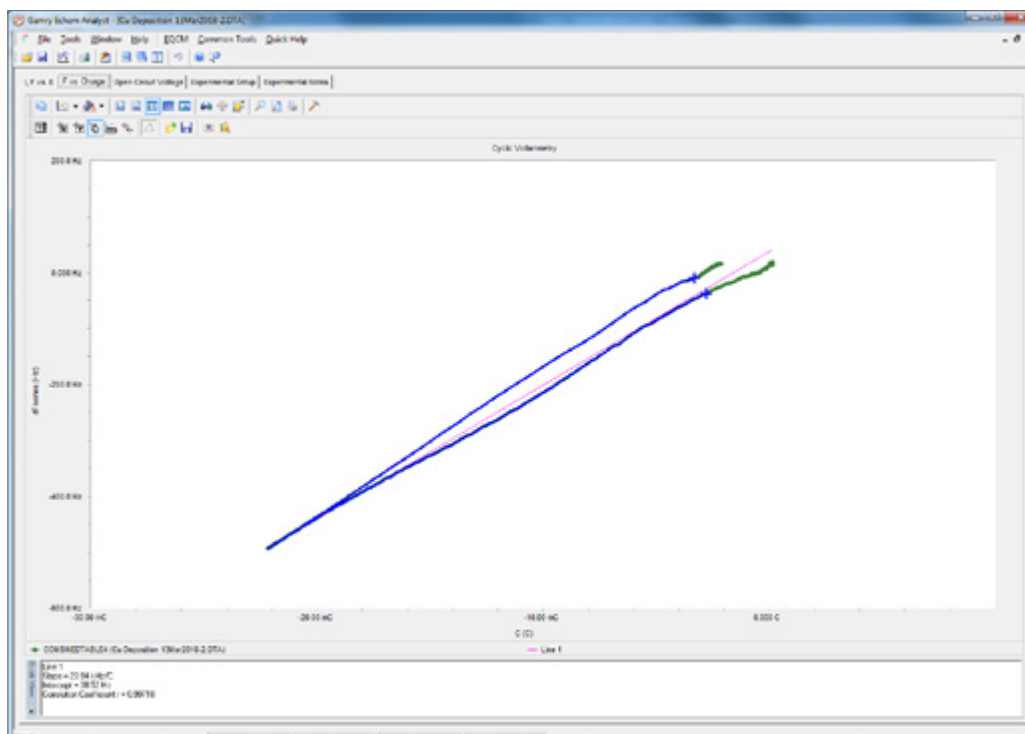


**Figure 16.** Echem Analyst™ showing the linear fit of change the bottom of the window.

The calibration factor for the crystal is then calculated according to equation 7:

$$C_f = \frac{\text{Slope} \times F \times EA \times n}{MM_{Cu} \times 10^6} \quad 7$$

where  $F$  is the Faraday Constant,  $EA$  is the electroactive area,  $MM_{Cu}$  is the molar mass of Cu, and  $n$  is the number of electrons. The  $10^6$  is used to convert from grams to micrograms.  $C_f$  is calculated to be 69.0 Hz cm<sup>2</sup>/μg. This is approximately 20% higher than the theoretical value of 56.6 Hz cm<sup>2</sup>/μg.

If you already know your calibration factor accurately you can determine the molar mass of the mobile species (deposited, in this instance) during your experiment. Use the **Curve Selector** to plot change in mass ( $\Delta M$ ) versus charge as shown in Figure 17.

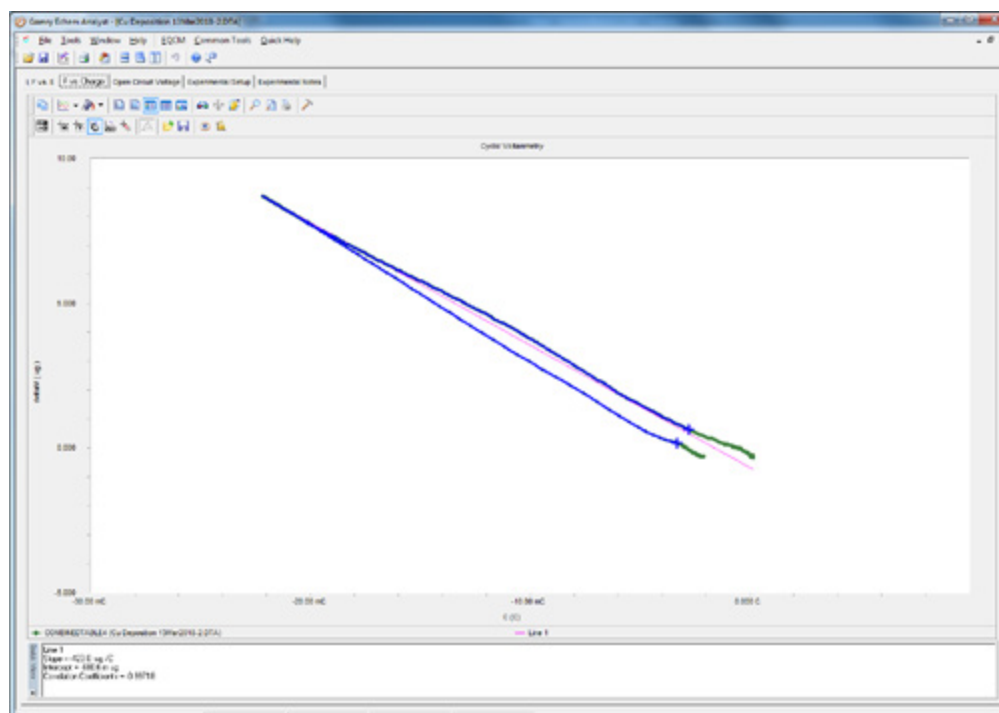
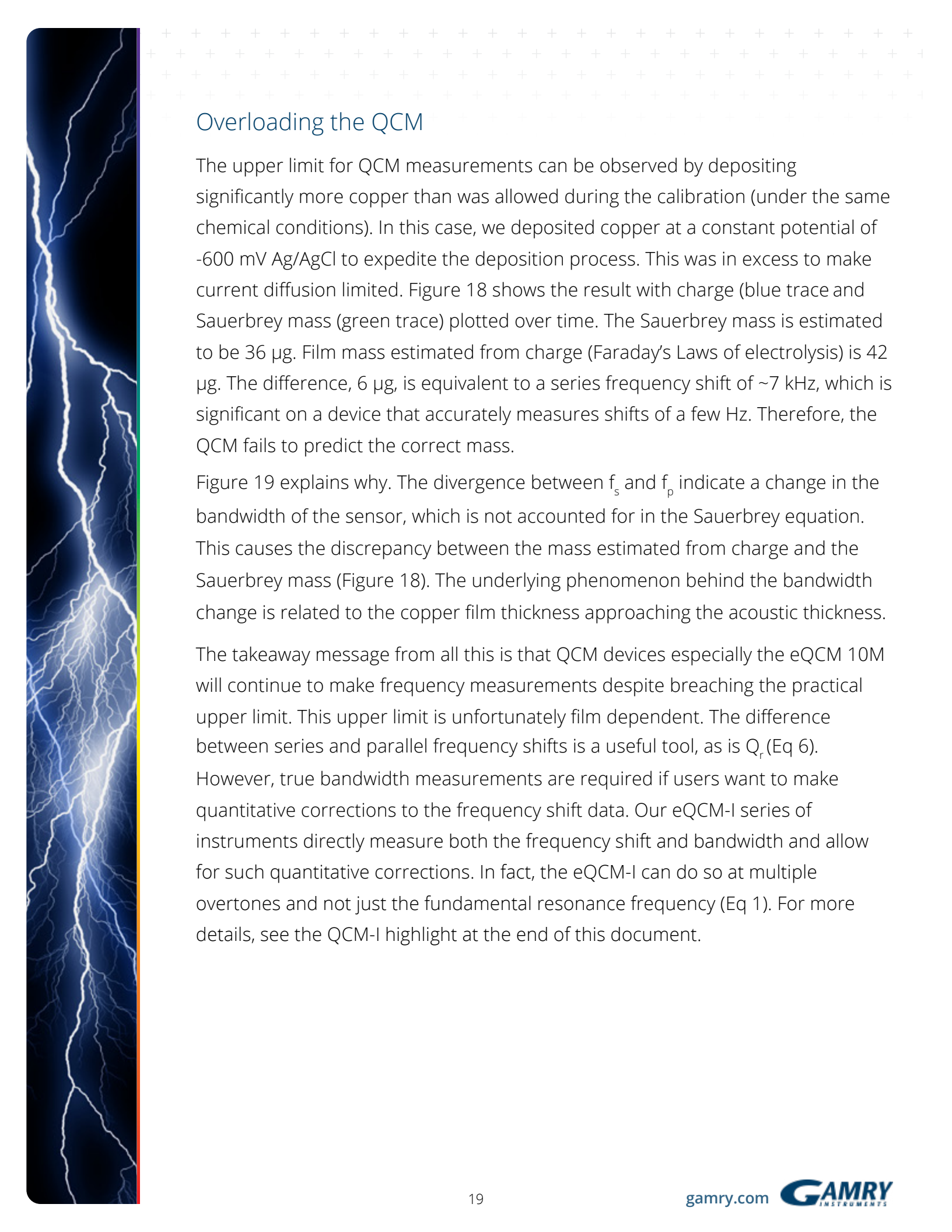


**Figure 17.** Echem Analyst showing the linear fit for change in mass versus charge in the **Quick View** pane at the bottom of the window.

Echem Analyst uses the calibration factor entered into Resonator software, along with the electroactive area, to calculate the mass. The slope of the line, after performing a second linear fit, for the deposition is  $-361.8 \mu\text{g}/\text{C}$ . The molar mass of the  $\text{Cu}^{2+}$  can be calculated using equation 8

$$MM = \frac{|Slope| \times F \times n}{10^6} \quad 8$$

where  $F$  and  $n$  are as described previously. In this instance the molar mass was calculated to be  $69.8 \text{ g/mol}$ .

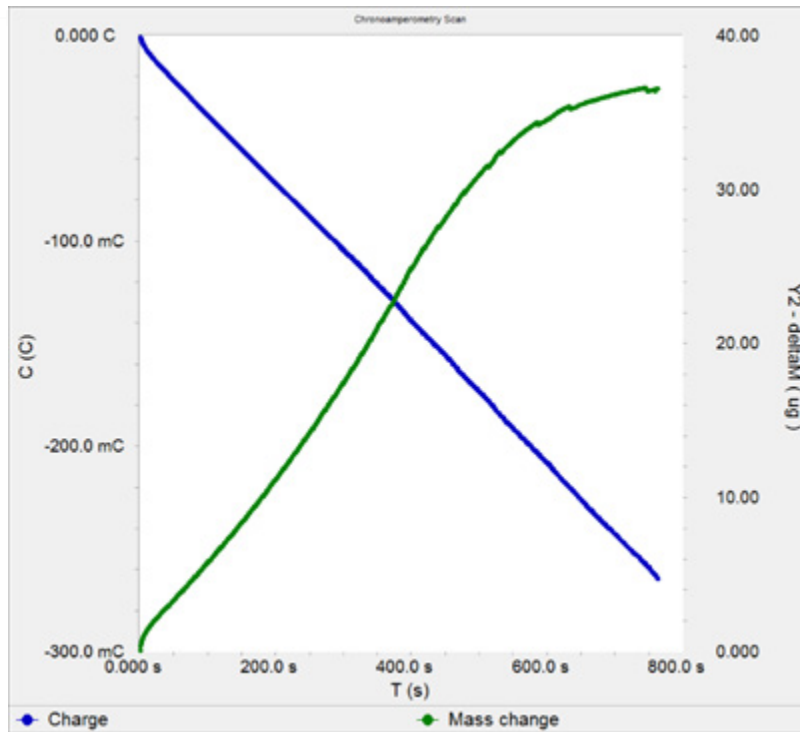


## Overloading the QCM

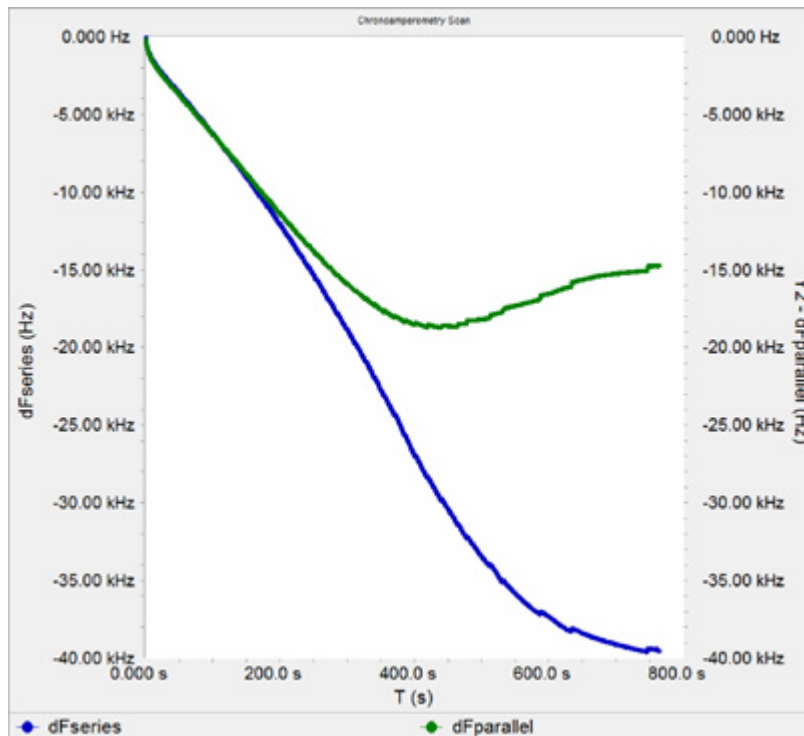
The upper limit for QCM measurements can be observed by depositing significantly more copper than was allowed during the calibration (under the same chemical conditions). In this case, we deposited copper at a constant potential of -600 mV Ag/AgCl to expedite the deposition process. This was in excess to make current diffusion limited. Figure 18 shows the result with charge (blue trace and Sauerbrey mass (green trace) plotted over time. The Sauerbrey mass is estimated to be 36  $\mu\text{g}$ . Film mass estimated from charge (Faraday's Laws of electrolysis) is 42  $\mu\text{g}$ . The difference, 6  $\mu\text{g}$ , is equivalent to a series frequency shift of  $\sim 7$  kHz, which is significant on a device that accurately measures shifts of a few Hz. Therefore, the QCM fails to predict the correct mass.

Figure 19 explains why. The divergence between  $f_s$  and  $f_p$  indicate a change in the bandwidth of the sensor, which is not accounted for in the Sauerbrey equation. This causes the discrepancy between the mass estimated from charge and the Sauerbrey mass (Figure 18). The underlying phenomenon behind the bandwidth change is related to the copper film thickness approaching the acoustic thickness.

The takeaway message from all this is that QCM devices especially the eQCM 10M will continue to make frequency measurements despite breaching the practical upper limit. This upper limit is unfortunately film dependent. The difference between series and parallel frequency shifts is a useful tool, as is  $Q_r$  (Eq 6). However, true bandwidth measurements are required if users want to make quantitative corrections to the frequency shift data. Our eQCM-I series of instruments directly measure both the frequency shift and bandwidth and allow for such quantitative corrections. In fact, the eQCM-I can do so at multiple overtones and not just the fundamental resonance frequency (Eq 1). For more details, see the QCM-I highlight at the end of this document.

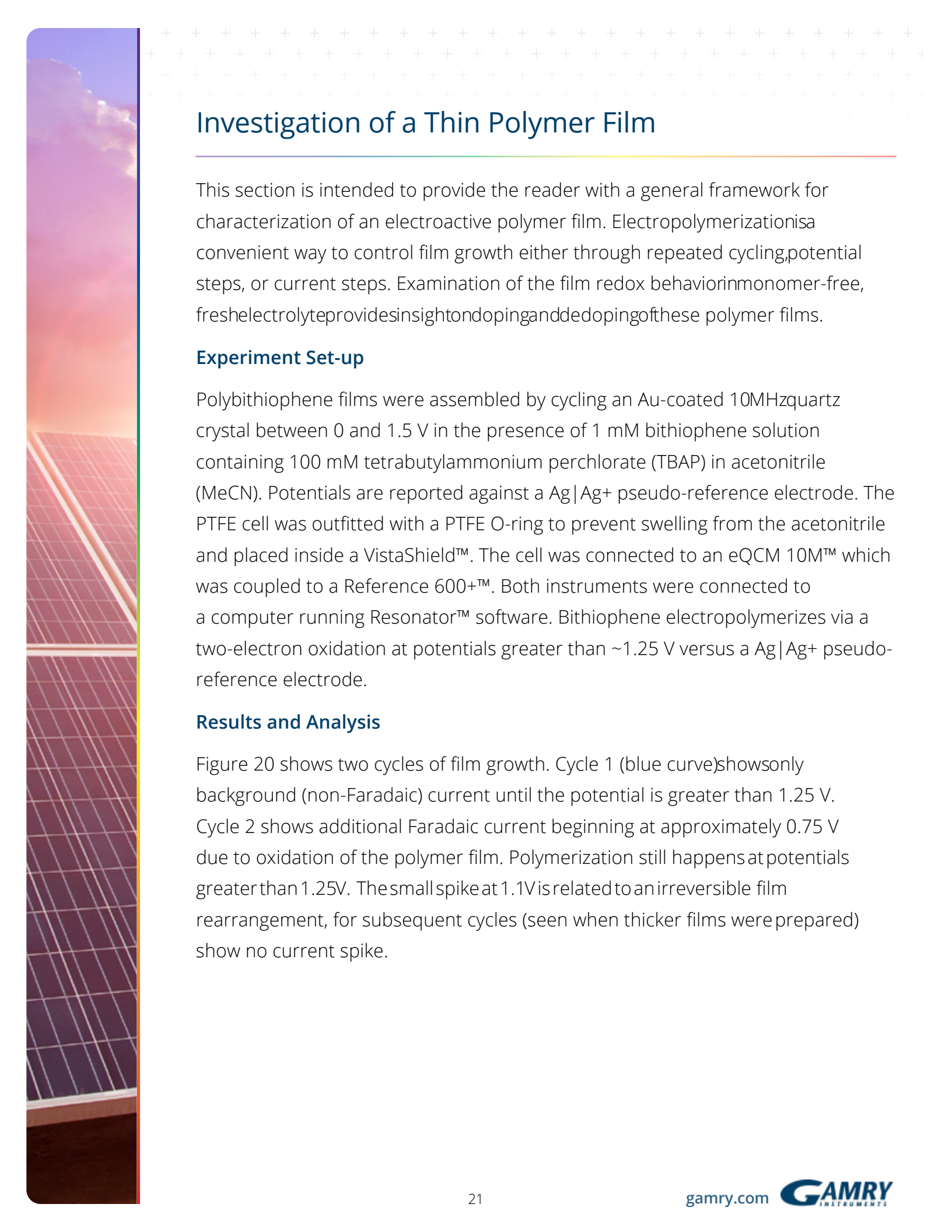


**Figure 18.** Charge passed and mass change vs. time.



**Figure 19.** Series and parallel frequency shifts vs. time.





## Investigation of a Thin Polymer Film

---

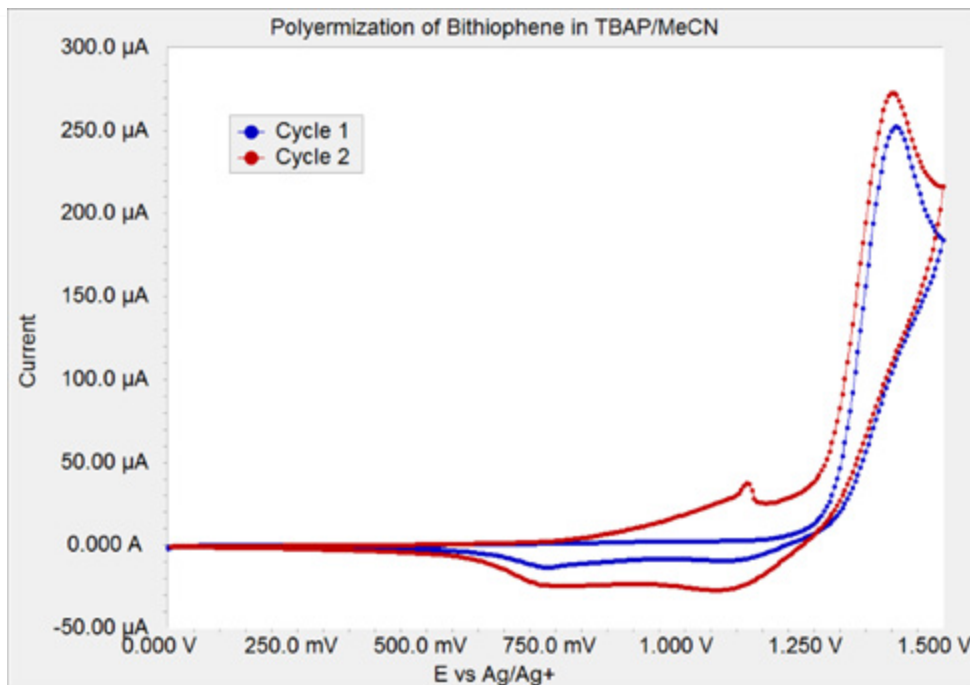
This section is intended to provide the reader with a general framework for characterization of an electroactive polymer film. Electropolymerization is a convenient way to control film growth either through repeated cycling, potential steps, or current steps. Examination of the film redox behavior in monomer-free, fresh electrolyte provides insight on doping and dedoping of these polymer films.

### Experiment Set-up

Polybithiophene films were assembled by cycling an Au-coated 10 MHz quartz crystal between 0 and 1.5 V in the presence of 1 mM bithiophene solution containing 100 mM tetrabutylammonium perchlorate (TBAP) in acetonitrile (MeCN). Potentials are reported against a Ag|Ag<sup>+</sup> pseudo-reference electrode. The PTFE cell was outfitted with a PTFE O-ring to prevent swelling from the acetonitrile and placed inside a VistaShield™. The cell was connected to an eQCM 10M™ which was coupled to a Reference 600+™. Both instruments were connected to a computer running Resonator™ software. Bithiophene electropolymerizes via a two-electron oxidation at potentials greater than ~1.25 V versus a Ag|Ag<sup>+</sup> pseudo-reference electrode.

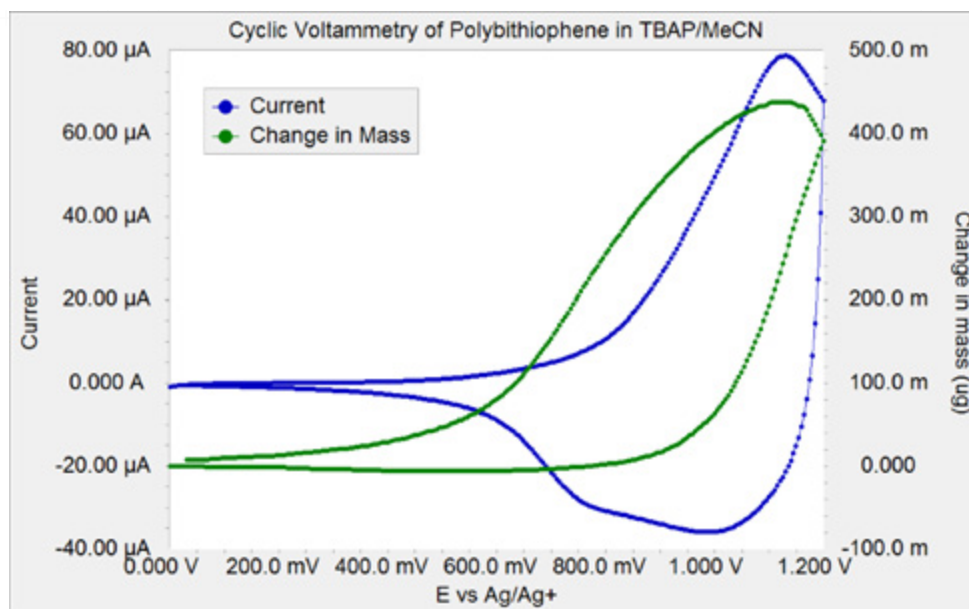
### Results and Analysis

Figure 20 shows two cycles of film growth. Cycle 1 (blue curve) shows only background (non-Faradaic) current until the potential is greater than 1.25 V. Cycle 2 shows additional Faradaic current beginning at approximately 0.75 V due to oxidation of the polymer film. Polymerization still happens at potentials greater than 1.25 V. The small spike at 1.1 V is related to an irreversible film rearrangement, for subsequent cycles (seen when thicker films were prepared) show no current spike.



**Figure 20.** Electropolymerization of 1 mM bithiophene in 0.1 M TBAP/MeCN. Scan rate was 50 mV/s.

After the film was deposited, the cell was washed with MeCN and then refilled with monomer-free electrolyte. Cycling of the polymer film revealed a broad-shaped couple at approximately 1 V (Figure 21). Mass increases during oxidation and decreases during reduction, respectively, yet does not return to the initial value indicating some loss of solvent, electrolyte, or polymer film.



**Figure 21.** Mass and current versus voltage for one cycle of polybithiophene in 0.1 M TBAP/MeCN. Scan rate was 100 mV/s.

Echem Analyst™ software calculates mass changes based on the change in series resonant frequency, using the rewritten Sauerbrey equation **9** below:

$$\Delta m = \frac{-\Delta f}{C_f} \quad \text{9}$$

where  $\Delta f$  is the change in  $f_s$  and  $C_f$  is the theoretical calibration factor,  $226 \text{ Hz cm}^2/\mu\text{g}^1$  for a 10 MHz AT-cut quartz crystal. Mass change plotted against charge for a cycle in monomer-free electrolyte reveals information about mobile species during oxidation and reduction. Figure 22 shows the change in mass ( $\Delta m$ ) versus the charge (C) for the first redox cycle.

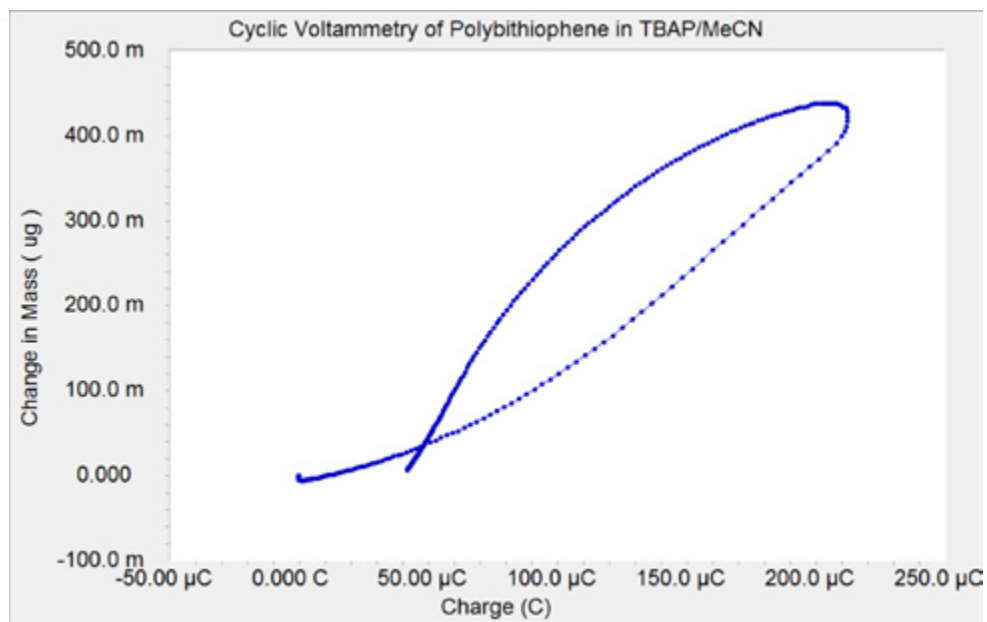


**Figure 22.** Change in mass versus charge for one redox cycle of polybithiophene in 0.1 M TBAP/MeCN. Scan rate was 100 mV/s.

The overall slope during oxidation is 1916  $\mu\text{g}/\text{C}$ . This can be converted to a molar mass by the following equation **10**

$$\text{Molar Mass} = \frac{|\text{Slope}| \times F \times n}{1 \times 10^6} \quad \text{10}$$

where  $F$  is Faraday's constant, and  $n$  is the number of electrons. Here  $n = 1$  because each thiophene in the polymer ring is being oxidized. The molar mass of 185 g/mol indicates that one perchlorate (99.5 g/mol) and approximately two molecules of MeCN (41 g/mol) enter the film for each electron that leaves the film.

Close examination of Figure 22 reveals differences in slope within the oxidation and reduction. Note that the beginning of the oxidation has a lower slope than the second half of the oxidation. Upon scan reversal, the slope is lower initially. Because electroneutrality must be maintained—one anion per electron—we can attribute these differences to differences in solvent ingress/egress. Solvent ingress is slower in the first part of the oxidation and the first part of the reduction.

Thicker polybithiophene films become viscous and swell when cycled in the presence of electrolyte. In these instances, mass measurements must be examined with a bit of skepticism because viscoelastic losses and density changes can also contribute to frequency changes. Tracking changes in  $f_p$  and  $Q_r$  (Eq 6) may be helpful in these cases. A more rigorous method to quantifying changes in viscoelasticity requires a QCM system that directly measures both frequency and bandwidth, such as our QCM-I series of instruments. For example, it is possible to construct the figure below (Figure 23) that compares a viscoelastic polymer film to both a rigid film and a theoretical viscous solution. Details on this method can be found in our [application notes here](#).

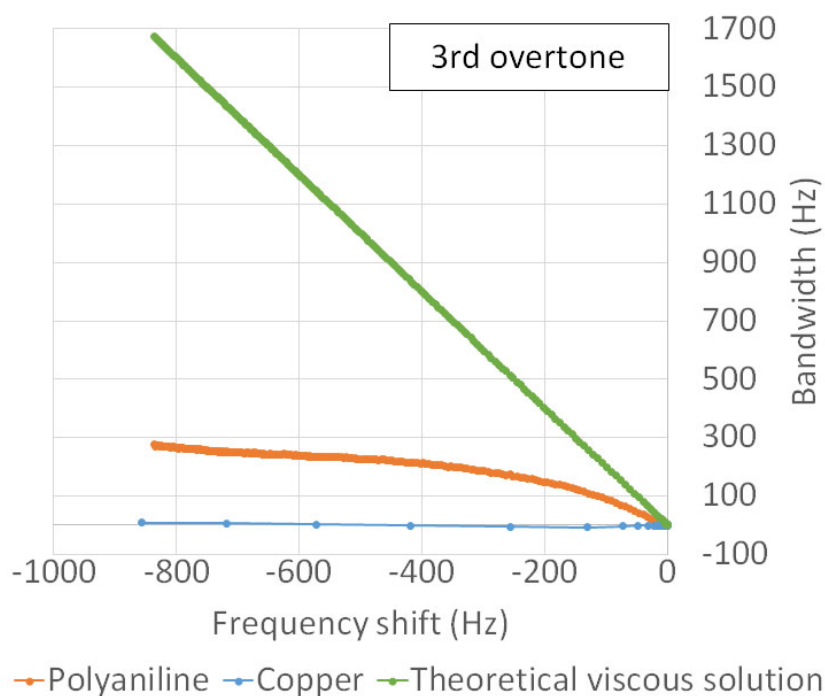


**Figure 23.** Bandwidth versus frequency shift for a viscoelastic polymer film (polyaniline) compared to a thin and rigid film (copper). A simple yet powerful graphical analysis that takes advantage of true bandwidth measurements

## System Information

The eQCM 10M is shipped with the Gamry Instruments Resonator software, Gamry Echem Analyst software, a Quick Start Guide, a Hardware Operator's Manual (CD), a Software Operator's Manual (CD), one EQCM cell, one AC Power Adapter, one USB

interface cable, one BNC cable, one potentiostat interface cable, and 5 Au-coated quartz crystals (5 MHz). The eQCM 10M is protected by a two-year factory service warranty.

The eQCM 10M must be connected to a computer with a Gamry Instruments potentiostat and a Physical Electrochemistry software license for incorporation and combination of QCM and potentiostat data into Echem Analyst. Microsoft® Windows® 7 or higher is required.

### eQCM 10M



### Specifications

Frequency range	1–10 MHz
Frequency resolution	0.02 MHz
Connection	USB
Operating temperature range	0–45°C
Relative humidity	maximum 90% non-condensing
Storage and shipping temperature	–25 to 75°C
Weight	1 kg
Dimensions	175 × 115 × 80 mm
AC power adapter	100–264 VAC, 47–63 Hz
Quartz-crystal microbalance	12 VDC, 25 W

## System Information

The QCM-I series of instruments are manufactured by MicroVacuum Ltd. (<http://www.owls-sensors.com/>) of Budapest, Hungary. MicroVacuum has integrated control of our potentiostats within the QCM-I software. Gamry has partnered with MicroVacuum for distribution of these instruments.

### QCM-I



The QCM-I unit is a high sensitivity mass sensor which measures the change in frequency of a quartz crystal resonator. As a label free biosensor, it measures the “wet mass” of the adsorbed layer in processes occurring at or near the sensor surface. The measuring principle is based on impedance analysis of the quartz crystal. The resonant frequency and the bandwidth of the resonant conductance curve are determined. The bandwidth or full width at half maximum (FWHM) is in direct correlation with the quality factor (Q) which is the inverse of the well-known dissipation (D).

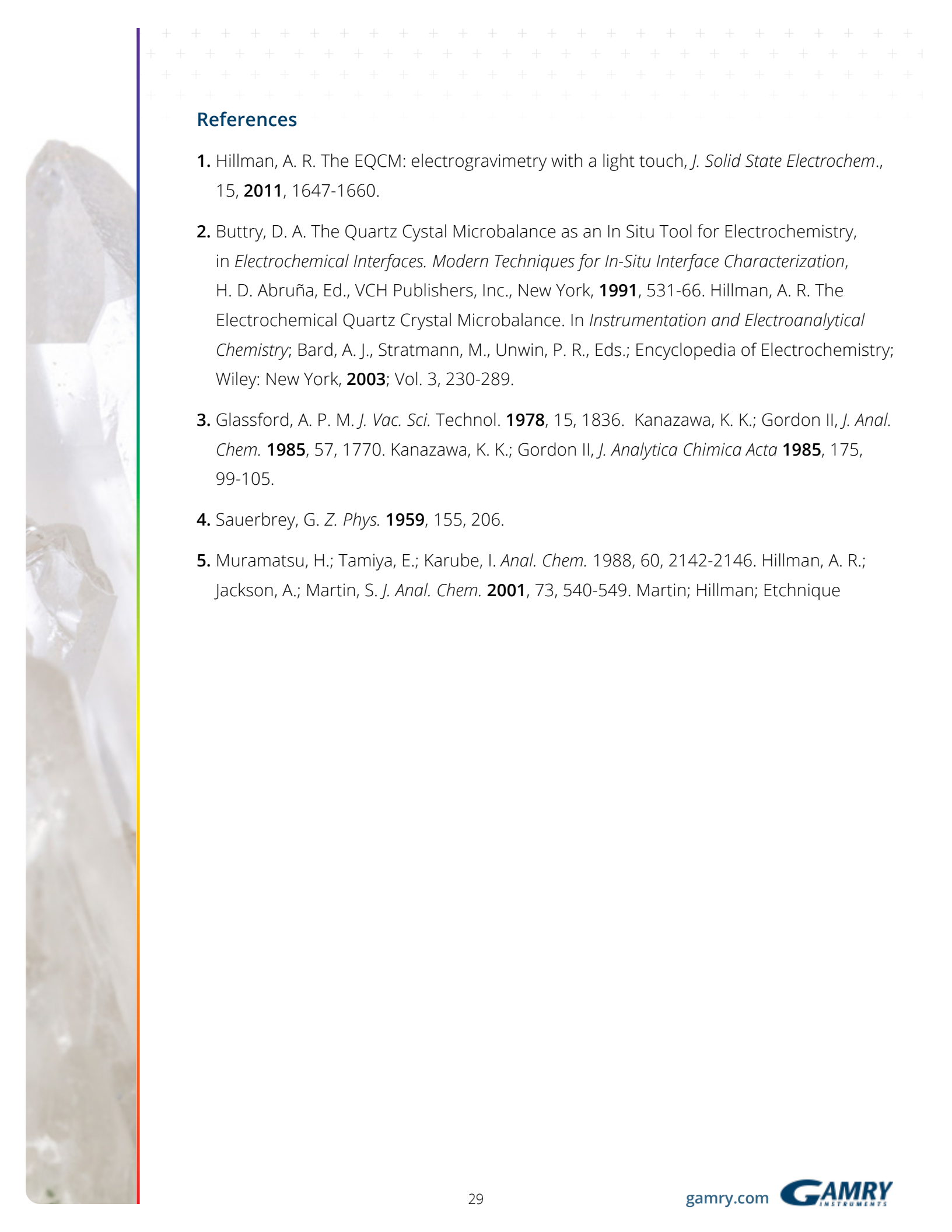
The QCM-I is shipped with a PC with the Biosense software installed, a Quick Start Guide, a Hardware Operator’s Manual, a Software Operator’s Manual, two QCM sensor holders, one sample injection system with semi-automatic injection valve, basic accessories, and on-site installation and training. The QCM-I is protected by a one-year factory service warranty. The QCM-I must be enabled for eQCM measurements and be connected to a computer with a Gamry Instruments potentiostat. Microsoft® Windows® 10 is required.



## QCM-I Specifications

Measurement Channels	2 (Upgradable to 4)
Frequency Range	0.05 – 80 MHz, up to the 13th overtone for a 5 MHz Crystal
Measurement Modes	Frequency Scan, Resonance Spectra, QCM(t), QCM(t)-EC, EC
Resonance Frequency sensitivity in Liquid	$\leq 2 \times 10^{-1}$ Hz
Dissipation Sensitivity in Liquid	$\leq 1 \times 10^{-7}$
Mass Sensitivity in Liquid *	$\leq 1 \text{ ng cm}^{-2}$
Parameters Recorded for each Overtone	Resonance Curve, Frequency, $\Delta$ Frequency, FWHM, $\Delta$ FWHM, Q, Dissipation, $\Delta$ Dissipation, Temperature, etc.
Thermal Zones	2, Independent Temperature Control
Working Temperature	4 °C to 80 °C with sample pre-equilibration on inlet
Temperature Stability	$<\pm 0.02$ °C
Temperature control	Set manually or via software
Flow Cell Volume	~ 40 $\mu$ l (typical with $\text{\O}14$ mm crystals)
Wetted Parts	PTFE, PEEK, SS, VITON (or Kalrez )
Sample Loading	Manual and Software Controlled Injection or Selector Valve
Pump	Peristaltic, Pulse-free Independent Flow Control on each Channel
Dimensions, weight	450 mm x 260 mm x185 mm, 5.5kg
PC Control	USB 2.0, Windows® 10
Power Supply	12VDC and 24VDC power supply with universal input voltage ( 100V-240V AC / 50-60 Hz )

\* Based on BioSense analysis using Sauerbrey equation and with data smoothing option enabled.



## References

1. Hillman, A. R. The EQCM: electrogravimetry with a light touch, *J. Solid State Electrochem.*, 15, **2011**, 1647-1660.
2. Buttry, D. A. The Quartz Crystal Microbalance as an In Situ Tool for Electrochemistry, in *Electrochemical Interfaces. Modern Techniques for In-Situ Interface Characterization*, H. D. Abruña, Ed., VCH Publishers, Inc., New York, **1991**, 531-66. Hillman, A. R. The Electrochemical Quartz Crystal Microbalance. In *Instrumentation and Electroanalytical Chemistry*; Bard, A. J., Stratmann, M., Unwin, P. R., Eds.; Encyclopedia of Electrochemistry; Wiley: New York, **2003**; Vol. 3, 230-289.
3. Glassford, A. P. M. *J. Vac. Sci. Technol.* **1978**, 15, 1836. Kanazawa, K. K.; Gordon II, *J. Anal. Chem.* **1985**, 57, 1770. Kanazawa, K. K.; Gordon II, *J. Analytica Chimica Acta* **1985**, 175, 99-105.
4. Sauerbrey, G. *Z. Phys.* **1959**, 155, 206.
5. Muramatsu, H.; Tamiya, E.; Karube, I. *Anal. Chem.* 1988, 60, 2142-2146. Hillman, A. R.; Jackson, A.; Martin, S. *J. Anal. Chem.* **2001**, 73, 540-549. Martin; Hillman; Etchnique



## Additional Resources

---

If you need additional information, please visit our website for our online resources and support.



### Technical Support

A compilation of technical support information by hardware and software.



### Software Updates

Licensed users can download the latest version of the Gamry Software.



### Documentation Downloads

Download manuals for hardware and software products.



### Electrochemistry Courses and Training

Information on short courses and electrochemistry training.



### Contact Technical Support

Get support from the electrochemical experts at Gamry.



### Support & Tutorial Videos

For all of our tutorial and support-related videos you can also visit Gamry Instruments YouTube



### Application Notes

A series of Application and Technical Notes to assist you in getting the most accurate results.



### Literature Database

A database of articles where people have used a Gamry System in their research

For help from our technical staff or questions  
about our products, please call us at **215-682-9330**,  
or send us an  **email**.

**Gamry.com**